IEEE Access
Multidisciplinary ⋮ Rapid Review ⋮ Open Access Journal

Received 14 June 2022, accepted 22 June 2022, date of publication 27 June 2022, date of current version 5 July 2022.

Digital Object Identifier 10.1109/ACCESS.2022.3186435

RESEARCH ARTICLE

Electronically Tunable Universal Filter and Quadrature Oscillator Using Low-Voltage Differential Difference Transconductance Amplifiers

MONTREE KUMNGERN[1], PICHAI SUKSAIBUL[1], FABIAN KHATEB[2,3,4], AND TOMASZ KULEJ[5]

[1]Department of Telecommunications Engineering, School of Engineering, King Mongkut's Institute of Technology Ladkrabang, Bangkok 10520, Thailand
[2]Department of Microelectronics, Brno University of Technology, 60190 Brno, Czech Republic
[3]Faculty of Biomedical Engineering, Czech Technical University in Prague, 27201 Kladno, Czech Republic
[4]Department of Electrical Engineering, Brno University of Defence, 66210 Brno, Czech Republic
[5]Department of Electrical Engineering, Czestochowa University of Technology, 42-201 Czestochowa, Poland

Corresponding author: Fabian Khateb (khateb@vutbr.cz)

This work was supported in part by the King Mongkut's Institute of Technology Ladkrabang under Grant KREF026201, and in part by the University of Defence Brno through the Organization Development Project VAROPS.

ABSTRACT This paper presents a new electronically tunable universal filter and quadrature oscillator for low frequency biomedical and biosensor applications employing low-voltage differential difference transconductance amplifier (DDTA). The DDTA CMOS structure uses 0.5 V of supply voltage and consumes 277 nW of power. Unlike the previous universal filters, the proposed filter provides many transfer functions of the standard five transfer functions such as low-pass, high-pass, band-pass, band-stop and all-pass with both unity and controlled voltage gains as well as both inverting and non-inverting transfer functions. The natural frequency and the voltage gain of the five standard transfer functions can be controlled electronically. For the band-pass filter, the third intermodulation distortion (IMD_3) was 0.37% for 20 mV_{pp} input signal while the output integrated noise was 61.37 μV. The dynamic range (DR) was 53.27 dB for 1% IMD_3. The quadrature oscillator has electronically and orthogonal control of the condition and frequency of oscillation. The proposed circuit and its applications were designed and verified via Cadence simulator tool using 0.13 μm UMC CMOS technology. Further, the circuit was evaluated by PSPICE simulation and experiment test using commercial OTA LM13700.

INDEX TERMS Universal filter, quadrature oscillator, differential difference transconductance amplifier, low-voltage, low-power CMOS.

I. INTRODUCTION

Universal filters are a useful block that usually provide five second-order transfer functions into a single topology such as low-pass (LPF), high-pass (HPF), band-pass (BPF), band-stop (BSF) and all-pass (APF) transfer functions. The second-order filters can be applied to FM stereo demodulation [1], audio crossover network circuit [2], programmable universal filter as commercial ICs [3] and high-order filters [4]–[7].

The oscillator circuits are the systems that usually generate a sinusoidal signal, which can be applied in telecommunication, control and measurement systems such as single sideband generator [1] and voltage-controlled oscillator of a phase-locked loop [8]. In addition, quadrature oscillators are the systems that usually provide two sinusoidal signals with 90° phase difference, which can be applied to quadrature mixer [9], phase sensitive detector [10], vector generators and selective voltmeters [11]. In these applications, it is

The associate editor coordinating the review of this manuscript and approving it for publication was Ludovico Minati.

advantageous if a single circuit can serve as a universal filter or a quadrature oscillator. In addition, the universal filter and oscillator, which are implemented as a single integrated circuit (IC), can help circuit designers to easily find the required integrated circuits.

Therefore, there are universal filters and sinusoidal oscillators that can be realized from a single topology available in literature [12]–[31]. These topologies can offer either a universal filter or an oscillator by slightly changing the connection [12]–[26], adjusting the ratio of circuit components [27]–[30], or programing techniques [31]. However, these topologies are realized based on high power consumption active devices that unfit the ultra-low power biomedical and biosensor systems.

Nowadays, the low-power second-order filters can be used to realize high-order filters for biomedical and biosensor applications such as fourth-order low-pass filters [32]–[35] and band-pass filters [36]–[38] as well as the low-frequency oscillators that can be applied in the biomedical systems [39], [41]. The LPF can be applied to bio-signal acquisition system [32], BPF can be applied to bionic ears [59], BSF can reduce the effect of the power line interference [60], APF can be used to realize audio delay line for use in hearing aids [61], HPF, LPF and BSF are used for signal conditioning for biosensors [62]. The voltage-controlled oscillator can be applied to biosensors [63], [64].

Recently, low-voltage, low-power universal filters and quadrature oscillators have been reported [42]–[46]. In [42], low-voltage, low-power universal filter employing new active element, difference transconductance amplifiers (DDTA), has been presented. The circuit employs three DDTAs and two grounded capacitors that offers twenty filtering functions. In [43], [44], a universal filter and quadrature oscillator that can be realized from a single topology has been proposed. The circuit in [43] employs four multiple-input operational transconductance amplifiers and two grounded capacitors that can realize eleventh filtering functions, but the circuit uses 1.2 V of voltage supply and consumes of 96 μW of power. The circuit in [44] employs two DDTA and two grounded capacitors that uses 0.3 V of voltage supply and consumes 0.715 μW of power, but in case the circuit realizing a quadrature oscillator, the condition of oscillation is controlled by adjusting the ratio of two capacitors which is not ideal for integrated circuit implementation. The structures in [45], [46] provide only universal filter. It should be noted that the voltage gain of all universal filters in [42]–[46] cannot be controlled.

In this work a low-voltage, low-power universal filter and quadrature oscillator suitable for application of biomedical and biosensors has been proposed. The universal filter is based on low-voltage, low-power difference transconductance amplifiers that offers the advantages: (1) providing thirty-six filtering functions that cover both inverting and non-inverting standard filter responses such as LPF, HPF, BPF, BSF and APF, (2) offering both unity and controlled voltage gains of these standard filter responses, (3) offering a high-input impedance, hence no additional buffer circuits are required, (4) providing electronic tuning capability of natural frequency, (5) offering the orthogonal control of natural frequency and quality factor. The quadrature oscillator can be realized by slightly modifying the proposed universal filter. The condition and frequency of oscillations can be orthogonally and electronically controlled. The output terminals possess low-impedance level which can be connected directly to a load without additional buffer circuit.

II. PROPOSED CIRCUIT

A. LOW-VOLTAGE DDTA

Fig. 1 shows the electrical symbol of the DDTA. The input and output ideal characteristic can be given by

$$\left.\begin{aligned} V_w &= V_{y1} - V_{y2} + V_{y3} \\ I_o &= g_m\left(V_w - V_{y4}\right) \end{aligned}\right\} \tag{1}$$

where V_{y1}, V_{y2}, V_{y3}, V_{y4} are the input voltages, V_w is the output voltage, I_o is the output current, and g_m is the transconductance gain. It should be noted that this device offers the output voltage of addition and subtraction voltages as w-terminal and the output current of addition and subtraction voltages as o-terminal.

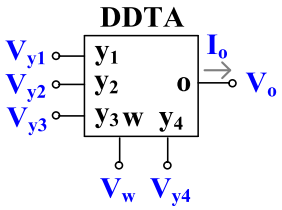

FIGURE 1. Electrical symbol of DDTA.

The innovative low-voltage DDTA CMOS structure was firstly presented in [44]. The modifications presented in this paper, compared with [44], are shown and highlighted in Fig. 2 a) the symbol and realization of the multiple-input MOS transistor (MI-MOST) is shown in b) and c), respectively. The original structure comprised of the differential-difference current conveyor (DDCC) and the transconductance amplifier (TA). The circuit employed several non-conventional techniques: 1) the partial positive feedback (M_7, M_8) that creates a negative conductance boosting the gain of the DDCC [47], 2) the bulk-driven non-tailed differential stages ($M_{1A,1B}$, $M_{2A,2B}$, M_3, M_4. M_5, M_6) that enable rail-to-rail operation under extremely low voltage supply ($\leq$ 0.5V) [48], [49], [50], 3) multiple-input technique MI-MOST for the DDCC (M_{1A}, M_{2B}) that simplify the structure by reducing the number of the differential pairs from standard two to one [51], [52], and 4) the linear resistor R used for optimum linearity of the TA [53]. However, along with the above-mentioned techniques, additional techniques have been used in the presented structure, in order to enhance the performance of this active element, i.e. the super class AB stage [54] and the self-cascoded MOS transistor [55] have

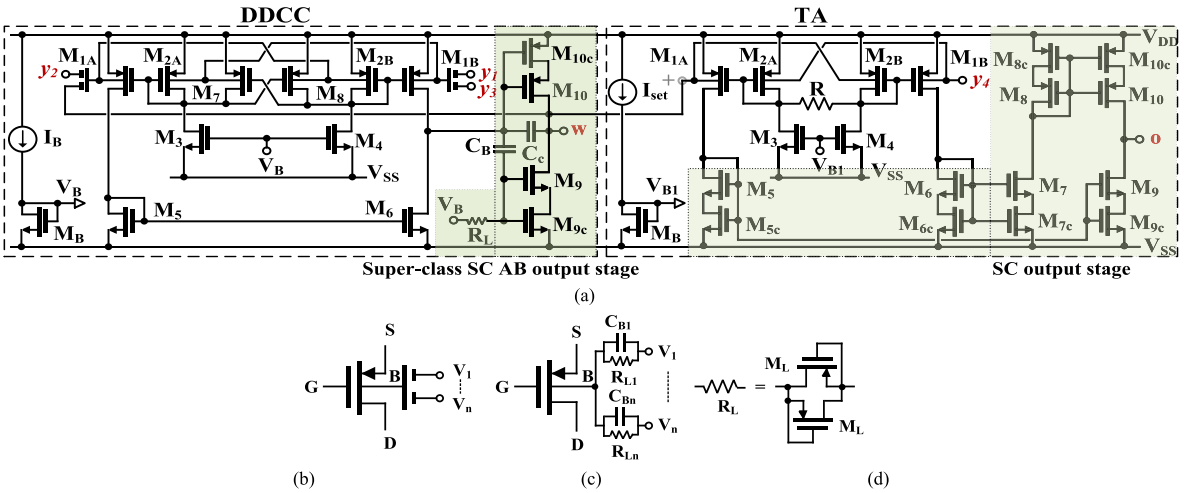

FIGURE 2. The DDTA: a) the modified CMOS structure, b) symbol, c) the realization of the MI-MOST, and d) the realization of the R_L.

been used. The self-cascoded transistor is very suitable solution for circuits with low-voltage supply (≈0.5V) since one transistor operates in saturation while the second one in linear region that results in drain-source voltage of both transistor close to the drain-source voltage of a single transistor while with much increased output resistance. In Fig. 2 a) for the DDCC block and in order to achieve power efficient class AB output stage of the DDCC a super class AB stage is used. This stage is simply obtained by using the capacitor C_B that for ac operation boosts the dynamic current above the quiescent current that is settled by the high resistance R_L by connecting the gate of $M_9$to the bias voltage V_B. The high resistance R_L is realized by two turned off diodes created by two identical MOS transistors M_R as shown in Fig. 2 d). For the high linear TA that suffered from low output resistance value, which was around 5.1 MΩ [44], the self-cascode transistors M_5, M_{5c}-M_{10}, M_{10c} that significantly increase the output resistance up to 1.18 GΩ has been used. Note that none of the super class AB stage or the self-cascode technique consume extra power, which is a benefit. Also, note that the low output resistance value of the TA caused degraded attenuation at low frequency for the filter function like HPF and BPF [44]. It is worth mentioning that the optimum linearity for TA is achieved when $g_m = 1/R$ [53]. Therefore, TA with large transconductance value means low R and low chip area and vice versa.

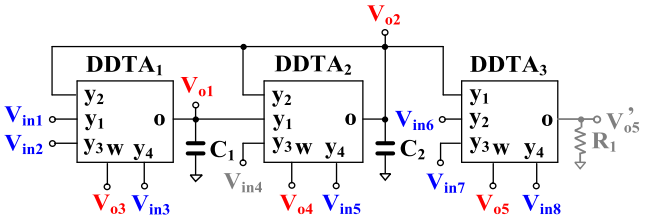

FIGURE 3. Proposed multiple-input multiple-output universal filter.

B. MULTIPLE-INPUT MULTIPLE-OUTPUT UNIVERSAL FILTER

The proposed universal filter employing three DDTAs, two grounded capacitors and one grounded resistor is shown

$$V_{o1} = \frac{\{(sC_2g_{m1} + g_{m1}g_{m2})(V_{in1} + V_{in2} - V_{in3}) - g_{m1}g_{m2}(V_{in4} - V_{in5})\}}{s^2C_1C_2 + sC_1g_{m2} + g_{m1}g_{m2}} \tag{2}$$

$$V_{o2} = \frac{g_{m1}g_{m2}(V_{in1} + V_{in2} - V_{in3}) + sC_2g_{m1}(V_{in4} - V_{in5})}{s^2C_1C_2 + sC_1g_{m2} + g_{m1}g_{m2}} \tag{3}$$

$$V_{o3} = \frac{\left(s^2C_1C_2 + sC_2g_{m1}\right)(V_{in1} + V_{in2} - V_{in3}) - sC_1g_{m2}(V_{in4} - V_{in5})}{s^2C_1C_2 + sC_1g_{m2} + g_{m1}g_{m2}} \tag{4}$$

$$V_{o4} = \frac{sC_2g_{m1}(V_{in1} + V_{in2} - V_{in3}) + s^2C_1C_2(V_{in4} - V_{in5})}{s^2C_1C_2 + sC_1g_{m2} + g_{m1}g_{m2}} \tag{5}$$

$$V_{o5} = \frac{V_{o2} - V_{in6} + V_{in7}}{s^2C_1C_2 + sC_1g_{m2} + g_{m1}g_{m2}} \tag{6}$$

$$\left.\begin{aligned} V'_{o5} &= \frac{g_{m3}R_1(V_{o2} - V_{in6} + V_{in7} - V_{in8})}{s^2C_1C_2 + sC_1g_{m2} + g_{m1}g_{m2}} \\ V'_{o5} &= \frac{g_{m3}R_1(V_{o5} - V_{in8})}{s^2C_1C_2 + sC_1g_{m2} + g_{m1}g_{m2}} \end{aligned}\right\} \tag{7}$$

TABLE 1. Obtaining variant filtering functions of the proposed filter.

Filtering Function		Gain	Input condition	Output
LPF	Inverting	1	V_{in4} is supplied by the input signal	V_{o1}
	Non-inverting	1	V_{in5} is supplied by the input signal	V_{o1}
	Non-inverting	1	V_{in1} is supplied by the input signal	V_{o2}
	Non-inverting	1	V_{in2} is supplied by the input signal	V_{o2}
	Inverting	1	V_{in3} is supplied by the input signal	V_{o2}
	Non-inverting	$g_{m3}R_1$	V_{in1} is supplied by the input signal	V'_{o5}
	Non-inverting	$g_{m3}R_1$	V_{in2} is supplied by the input signal	V'_{o5}
	Inverting	$g_{m3}R_1$	V_{in3} is supplied by the input signal	V'_{o5}
BPF	Non-inverting	1	V_{in1} and V_{in4} are supplied together by the input signal	V_{o1}
	Non-inverting	1	V_{in4} is supplied by the input signal	V_{o2}
	Inverting	1	V_{in5} is supplied by the input signal	V_{o2}
	Inverting	1	V_{in4} is supplied by the input signal	V_{o3}
	Non-inverting	1	V_{in5} is supplied by the input signal	V_{o3}
	Non-inverting	1	V_{in1} is supplied by the input signal	V_{o4}
	Non-inverting	1	V_{in2} is supplied by the input signal	V_{o4}
	Inverting	1	V_{in3} is supplied by the input signal	V_{o4}
	Non-inverting	$g_{m3}R_1$	V_{in4} is supplied by the input signal	V'_{o5}
	Inverting	$g_{m3}R_1$	V_{in5} is supplied by the input signal	V'_{o5}
HPF	Non-inverting	1	V_{in1} and V_{in4} are supplied together by the input signal	V_{o3}
	Non-inverting	1	V_{in2} and V_{in4} are supplied by the input signal	V_{o3}
	Inverting	1	V_{in3} and V_{in5} are supplied by the input signal	V_{o3}
	Non-inverting	1	V_{in4} is supplied by the input signal	V_{o4}
	Inverting	1	V_{in5} is supplied by the input signal	V_{o4}
	Inverting	$g_{m3}R_1$	V_{in1}, V_{in4}, V_{in6} are supplied together by the input signal	V'_{o5}
	Non-Inverting	$g_{m3}R_1$	V_{in3}, V_{in5}, V_{in7} are supplied together by the input signal	V'_{o5}
BSF	Inverting	1	V_{in4}, V_{in6} are supplied together by the input signal	V_{o5}
	Non-inverting	1	V_{in5} and V_{in7} are supplied together by the input signal	V_{o5}
	Inverting	$g_{m3}R_1$	V_{in4} and V_{in8} are supplied together by the input signal	V'_{o5}
	Inverting	$g_{m3}R_1$	V_{in4} and V_{in6} are supplied together by the input signal	V'_{o5}
	Non-inverting	$g_{m3}R_1$	V_{in5} and V_{in7} are supplied together by the input signal	V'_{o5}
APF	Inverting	1	V_{in4} and V_{in6} are supplied together by the input signal and V_{in7} is connected to V_{o2}	V_{o5}
	Inverting	1	V_{in4} and V_{in8} are supplied together by the input signal and V_{in7} is connected to V_{o2}	V_{o5}
	Non-inverting	1	V_{in5} and V_{in7} are supplied together by the input signal and V_{in6} is connected to V_{o2}	V_{o5}
	Non-inverting	1	V_{in5} and V_{in7} are supplied together by the input signal and V_{in8} is connected to V_{o2}	V_{o5}
	Inverting	$g_{m3}R_1$	V_{in4} and V_{in6} are supplied together by the input signal and V_{in7} is connected to V_{o2}	V'_{o5}
	Non-inverting	$g_{m3}R_1$	V_{in5} and V_{in7} are supplied together by the input signal and V_{in6} is connected to V_{o2}	V'_{o5}

Note: The input terminals that are not supplied by signals are grounded.

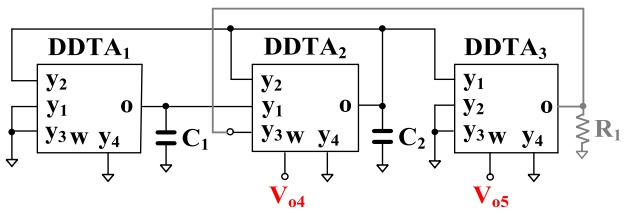

FIGURE 4. Modified quadrature oscillator.

in Fig. 3. The circuit has eight input terminals with high-impedance level and six output terminals. Thus, the input terminals can be connected to any terminals without buffer circuit requirements. Using (1) and nodal analysis, the output voltages of Fig. 3 can be expressed as (2)–(7), shown at the bottom of the previous page. From (2)-(7), the five standard filtering responses such as LPF, HPF, BPF, BSF and APF can be achieved by appropriately applying the input signals and suitable connecting output terminals as shown in Table 1. It can be seen from Table 1 that the five standard filtering responses possess both non-inverting and inverting transfer functions as well as both unity and controlled voltage gain of the transfer functions. The proposed topology offers thirty-six filtering responses. The natural frequency (ω_o), the quality factor (Q) of filters can be given by

$$\omega_o = \sqrt{\frac{g_{m1}g_{m2}}{C_1C_2}} \tag{8}$$

$$Q = \sqrt{\frac{g_{m2}C_1}{g_{m1}C_2}} \tag{9}$$

The voltage gain of transfer function can be given by

$$H_o = g_{m3}R_1 \tag{10}$$

From (8) and (9) the quality factor can be given by C_1/C_2 by letting $g_{m1} = g_{m2}$ whereas the natural frequency can be obtained electronically by adjusting g_m ($g_m = g_{m1} = g_{m2}$). Therefore, the natural frequency and the quality factor can be orthogonally controlled. From (10), the voltage gain can be controlled electronically by g_{m3} and constant R_1.

C. MODIFIED QUADRATURE OSCILLATOR

Fig. 4 shows the modified quadrature oscillator using the proposed universal filter in Fig. 3. The non-inverting BPF having the voltage gain of Fig. 3 is used for creating the loop-gain of the oscillator. Considering the output V'_{o5} and the input V_{in4}, the transfer function of the non-inverting BPF can be expressed by

Note: The input terminals that are not supplied by signals are grounded.

$$\frac{V'_{o5}}{V_{in4}} = \frac{(g_{m3}R_1)\,(sC_2g_{m1})}{s^2C_1C_2 + sC_2g_{m1} + g_{m1}g_{m2}} \tag{11}$$

Letting $V'_{o5}/V_{in4} = 1$, the characteristic equation of the oscillator can be given by

$$s^2C_1C_2 + sC_2g_{m1}\,(1 - g_{m3}R_1) + g_{m1}g_{m2} = 0 \tag{12}$$

The condition of oscillation (CO) and the frequency of oscillation (FO) of the oscillator can be given respectively by

$$g_{m3}R_1 = 1 \tag{13}$$

$$\omega_o = \sqrt{\frac{g_{m1}g_{m2}}{C_1C_2}} \tag{14}$$

The CO can be controlled electronically by g_{m3} and the FO can be controlled electronically by g_{m2}. The capacitor C_1 can also be used to adjust the FO if required. Thus the CO and FO of the quadrature oscillation can be independently controlled.

D. NON-IDEALITIES ANALYSIS

Considering non-idealities of DDTA, (1) can be rewritten as

$$\left.\begin{aligned} V_w &= \beta_{j1}V_{y1} - \beta_{j2}V_{y2} + \beta_{j3}V_{y3} \\ I_o &= g_{mnj}V_w \end{aligned}\right\} \tag{15}$$

where $\beta_{j1} = 1 - \varepsilon_{j1v}$ and $\varepsilon_{j1v}(|\varepsilon_{j1v}| \ll 1)$ denotes the voltage tracking error from V_{y1} to V_w of j-th DDTA, $\beta_{j2} = 1 - \varepsilon_{j2v}$ and $\varepsilon_{j2v}(|\varepsilon_{j2v}| \ll 1)$ denotes the voltage tracking error from V_{y2} to V_w of j-th DDTA and $\beta_{j3} = 1 - \varepsilon_{j3v}$ and $\varepsilon_{j3v}(|\varepsilon_{j3v}| \ll 1)$ denotes the voltage tracking error from V_{y2} to V_w of j-th DDTA. The non-ideal transconductance gain g_{mnj} can be given by

$$g_{mnj}\,(s) = \left(\frac{\omega_{gmj}}{s + \omega_{gmj}}\right) g_{mj} \tag{16}$$

where ω_{gmj} and g_{mj} denote the first-order pole frequency and the open-loop transconductance gain of j-th DDTA.

The non-ideal transconductance gain of DDTA is caused by the parasitic capacitor and parasitic resistor at o-terminal. In the frequency range that generates these parasitic capacitance and resistance, g_{mnj} can be modified as [56] (17)–(23), shown at the bottom of the page.

Using (17), the denominator of (18)-(23) can be expressed by (24), as shown at the bottom of the next page.

From (24), the non-idealities of the DDTAs affect the circuit characteristics, which depart from ideal values. The parasitic effects from the DDTA can be made negligible by

$$g_{mnj}\,(s) \cong g_{mj}\left(1 - \mu_j s\right) \tag{17}$$

where $\mu_j = 1/\omega_{gmj}$.

$$V_{o1} = \frac{\{(sC_2g_{m1} + g_{mn1}g_{mn2}\beta_{22})\,(\beta_{11}V_{in1} + \beta_{13}V_{in2} - V_{in3}) - g_{mn1}g_{mn2}\,(\beta_{12}\beta_{23}V_{in4} - V_{in5})\}}{s^2C_1C_2 + sC_1g_{mn2}\beta_{22} + g_{mn1}g_{mn2}\beta_{12}\beta_{21}} \tag{18}$$

$$V_{o2} = \frac{\left\{g_{mn1}g_{mn2}\beta_{21}\left(\beta_{11}V_{in1} + \beta_{13}V_{in2} - V_{in3}\right) + sC_2g_{mn1}\,(\beta_{23}V_{in4} - V_{in5})\right\}}{s^2C_1C_2 + sC_1g_{mn2}\beta_{22} + g_{mn1}g_{mn2}\beta_{12}\beta_{21}} \tag{19}$$

$$V_{o3} = \frac{\left\{\left(s^2C_1C_2 + sC_1g_{mn2}\beta_{22}\right)\left(\beta_{11}V_{in1} + \beta_{13}V_{in2} - V_{in3}\right) - sC_1g_{mn2}\,(\beta_{12}\beta_{23}V_{in4} - V_{in5})\right\}}{s^2C_1C_2 + sC_1g_{mn2}\beta_{22} + g_{mn1}g_{mn2}\beta_{12}\beta_{21}} \tag{20}$$

$$V_{o4} = \frac{\left\{sC_2g_{mn1}\beta_{11}\left(\beta_{21}V_{in1} + \beta_{13}V_{in2} - V_{in3}\right) + s^2C_1C_2\,(\beta_{23}V_{in4} - V_{in5})\right\}}{s^2C_1C_2 + sC_1g_{mn2}\beta_{22} + g_{mn1}g_{mn2}\beta_{12}\beta_{21}} \tag{21}$$

$$V_{o5} = \frac{\beta_{31}V_{o2} - \beta_{32}V_{in6} + \beta_{33}V_{in7} - V_{in8}}{s^2C_1C_2 + sC_1g_{mn2}\beta_{22} + g_{mn1}g_{mn2}\beta_{12}\beta_{21}} \tag{22}$$

$$\left.\begin{aligned} V'_{o5} &= \frac{g_{mn3}R_1(\beta_{31}V_{o2} - \beta_{32}V_{in6} + \beta_{33}V_{in7} - V_{in8})}{s^2C_1C_2 + sC_1g_{mn2}\beta_{22} + g_{mn1}g_{mn2}\beta_{12}\beta_{21}} \\ V'_{o5} &= \frac{g_{mn3}R_1(V_{o5} - V_{in8})}{s^2C_1C_2 + sC_1g_{mn2}\beta_{22} + g_{mn1}g_{mn2}\beta_{12}\beta_{21}} \end{aligned}\right\} \tag{23}$$

satisfying the following condition

$$\frac{C_2 g_{m1}\mu_1\beta_{22} - g_{m1}g_{m2}\mu_1\mu_2\beta_{12}\beta_{21}}{C_1C_2} \ll 1 \quad (25)$$

$$\frac{g_{m1}g_{m2}\mu_1\beta_{12}\beta_{21} + g_{m1}g_{m2}\mu_2\beta_{12}\beta_{21}}{C_2 g_{m1}\beta_{22}} \ll 1 \quad (26)$$

Therefore, the non-ideal natural frequency (ω_{on}) and the quality factor (Q_n) can be obtained respectively by

$$\omega_{on} = \sqrt{\frac{g_{m1}g_{m2}\beta_{12}\beta_{21}}{C_1C_2}} \quad (27)$$

$$Q_n = \frac{1}{\beta_{22}}\sqrt{\frac{C_1 g_{m2}\beta_{12}\beta_{21}}{C_2 g_{m1}}} \quad (28)$$

If p such as ω_{on} or Q_n is a function of x such as capacitor C or g_m, the sensitivity of a parameter $p$to an element x is given by [57]

$$S_x^p = \frac{x}{p}\frac{\partial p}{\partial x} = \frac{\partial(\ln p)}{\partial(\ln x)} \quad (29)$$

Using (29), the sensitivity of ω_{on} and Q_n with respect to circuit components and non-ideal parameters can be expressed by

$$S_{g_{m1}}^{\omega_{on}} = S_{g_{m2}}^{\omega_{on}} = S_{\beta_{12}}^{\omega_{on}} = S_{\beta_{21}}^{\omega_{on}} = -S_{C_1}^{\omega_{on}} = -S_{C_2}^{\omega_{on}} = \frac{1}{2} \quad (30)$$

$$S_{\beta_{22}}^{Q_n} = -1 \quad (31)$$

$$S_{C_1}^{Q_n} = S_{g_{m2}}^{Q_n} = S_{\beta_{12}}^{Q_n} = S_{\beta_{21}}^{Q_n} = -S_{C_2}^{Q_n} = -S_{g_{m1}}^{Q_n} = -\frac{1}{2} \quad (32)$$

It can be concluded from (30)-(32) that all the sensitivities are within unity in magnitude. Thus, the proposed filter enjoys good active and passive sensitivities.

Re-considering the output V'_{o5} and the input V_{in4}, the modified BPF can be expressed by

$$\frac{V'_{o5}}{V_{in4}} = \frac{sC_2 g_{mn1}g_{mn3}R_1\beta_{23}\beta_{31}}{s^2C_1C_2 + sC_2 g_{mn1}\beta_{22} + g_{mn1}g_{mn2}\beta_{12}\beta_{21}} \quad (33)$$

Letting V'_{o5}/V_{in4} =1, the characteristic equation of oscillator can by modified as

$$s^2C_1C_2 + sC_2 g_{mn1}(\beta_{22} - g_{mn3}R_1\beta_{23}\beta_{31}) + g_{mn1}g_{mn2}\beta_{12}\beta_{21} = 0 \quad (34)$$

The modified CO and FO of oscillator can be expressed respectively by

$$\beta_{22} - g_{mn3}R_1\beta_{31}\beta_{23} = 0 \quad (35)$$

$$\omega_o = \sqrt{\frac{g_{mn1}g_{mn2}\beta_{12}\beta_{21}}{C_1C_2}} \quad (36)$$

From (35) and (36), the electronic tuning capability of the oscillator can easily compensate the non-idealities of DDTAs.

III. RESULTS

A. SIMULATION RESULTS

The circuit has been designed and simulated in Cadence environment using the 0.13 μm UMC CMOS technology. The transistors aspect ratio of the DDTA are listed in Tab. 2. The voltage supply was $\pm$0.25 V. The bias current I_B and the nominal value of the I_{set} = 50 nA. The nominal value power consumption of the DDTA is 277 nW. The frequency characteristics of the gain of the open loop DDCC (i.e. DDA) and the TA are shown in Fig. 5. The gain of the DDA and TA at low frequencies enjoy high value of 88 dB and 46.65 dB, due to the increased output resistance, caused by the partial positive feedback and the self-cascode techniques. The frequency characteristic of the output impedance of the TA is shown in Fig. 6. Thanks to the self-cascode technique, the resistance at low frequencies is increased to 1.18 GΩ. The gain of the DDA and TA at low frequencies enjoy high value of 88 dB and 46.65 dB, due to the increased output resistance, caused by the partial positive feedback and the self-cascode techniques. The frequency characteristic of the output impedance of the TA is shown in Fig. 6. Thanks to the self-cascode technique, the resistance at low frequencies is increased to 1.18 GΩ. The rail-to-rail operation capability in inverting and non-inverting configuration of the DDCC is shown in Fig. 7. It can be seen that the input range of DDTA is wide and near to the supply rails. Fig. 8 shows the relations of I_o and $g_m$versus input voltage $V_{y4} - V_w$ when the bias current I_{set} was varied. The wide input voltage range, rail-to-rail, and the good linearity are evident.

TABLE 2. Transistors aspect ratios and passive elements of the DDTA in Fig. 2.

Device	W/L (µm/µm)
M_{1A}, M_{2A}, M_{1B}, M_{2B}	20/3
M_7, M_8, M_3-M_6, M_{9c}, M_{11c}, M_{12c}, M_B	10/3
M_9, M_{11}, M_{12}	3×10/3
M_{10}	3×15/3
M_{10c}	15/3
M_{13}, M_{15}, M_{13c}, M_{15c}	3×5/6
M_{14}, M_{16}	3×15/6
M_{14c}, M_{16c}	15/6
M_L	1/4

$$D(s) = s^2C_1C_2\left(1 - \frac{C_2 g_{m1}\mu_1\beta_{22} - g_{m1}g_{m2}\mu_1\mu_2\beta_{12}\beta_{21}}{C_1C_2}\right) + sC_2 g_{m1}\beta_{22}\left(1 - \frac{g_{m1}g_{m2}\mu_1\beta_{12}\beta_{21} + g_{m1}g_{m2}\mu_2\beta_{12}\beta_{21}}{C_2 g_{m1}\beta_{22}}\right) + g_{m1}g_{m2}\beta_{12}\beta_{21} \quad (24)$$

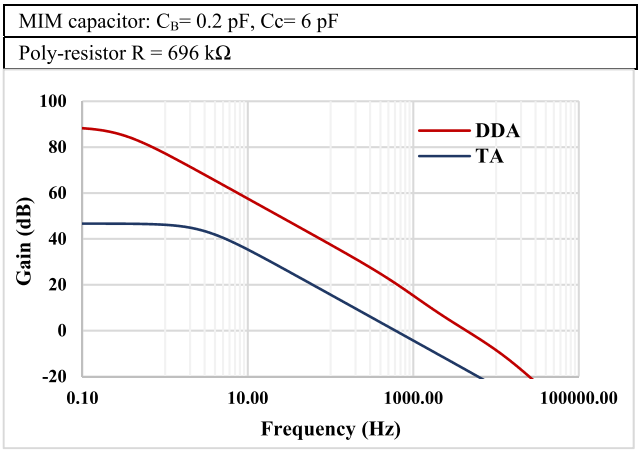

FIGURE 5. The frequency characteristic of the gain of the TA.

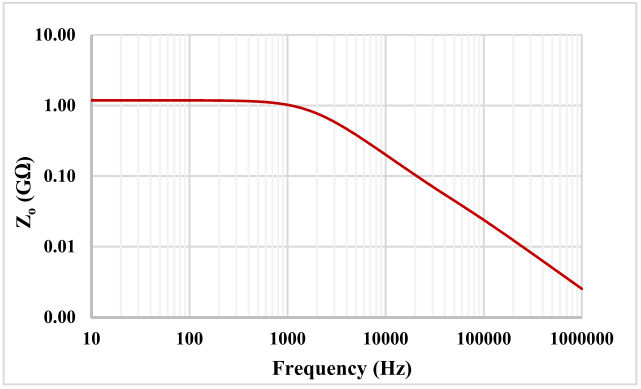

FIGURE 6. The frequency characteristic of the output impedance Z_o of the TA.

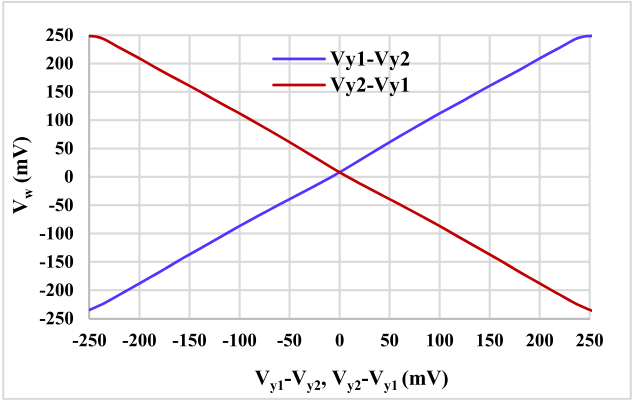

FIGURE 7. The relation between V_w and V_{y1}-V_{y2} and V_{y2}-V_{y1}.

For the filter application in Fig. 3, the off-chip components have the following values: C_1=C2 = 50 pF and R_1 = 12.9 MΩ Fig. 9 shows the frequency magnitude responses of LPF, HPF, BPF, BSF and APF. The natural frequency f_o was 231.7 Hz. Fig. 10 shows the frequency magnitude responses of BPF filter with different I_{set} = I_{set1} = I_{set2} =(30, 50, 70, 90, 110) nA while I_{set3} was fixed as 50 nA. The corresponding f_o was 131.8 Hz, 231.7 Hz, 338.84 Hz, 446.68 Hz and 562.34 Hz, respectively. Fig. 11 shows the frequency gain magnitude responses of BPF with different I_{set} = I_{set3} =(30, 50, 70, 90, 110) nA while I_{set1} and I_{set2} were fixed as 50 nA. The controlled gain was in range -4.6 dB, 0.07 dB, 3.1 dB, 5.4 dB, 7.24 dB. Further increase in gain could be obtained by increasing the R_1.

Fig. 12 shows the frequency magnitude responses of BP filter with process, voltage, temperature corners (PVT) and Monte Carlo (MC) analysis. The variation of process corners for MOS transistor were: slow-slow (SS), slow-fast (SF), fast-slow (FS) and fast-fast (FF), for voltage supply corners: 0.45V and 0.55V, for temperature corners were:−20 °C, 27 °C, 55 °C as shown in Fig. 12 (a), (b) and (c), respectively. A slight deviation can be seen for temperature corner 55 °C and this is expected due the operation of transistors in weak inversion region that is sensitive for temperature variation. The variation of the magnitude response of the BP filter with 200 runs MC is shown in Fig. 12 (d). The mean value of the gain is 0.13 dB and the standard deviation is 0.72 dB as shown in the histogram in Fig. 13.

To determine the third order intermodulation distortion IMD_3 of the BPF, two-tone test has been applied. The first tone was 10 mV_{pp} @ 220 Hz and the second one was 10 mV_{pp} @ 240 Hz. The spectrum of the output signal is shown in Fig. 14 indicating 0.37% IMD_3. The IMD_3 versus the input voltage V_{inpp} is shown in Fig. 15. The output noise of the BP filter is shown in Fig. 16. The RMS value integrated in the band pass was calculated to 61.37 μV. The dynamic range (DR) of the BP filter is then calculated as 53.27 dB for 1% IMD_3.

For the oscillator application in Fig. 4, the components had the following values: $C_1 = C_2$ =50 pF and R_1 = 14 MΩ. The starting oscillation and the steady state are shown in Fig. 17 (a) and (b).The V_{o4} and V_{o5} oscillation frequency is 238 kHz and total harmonic distortion (THD) 1% and 1.1%, respectively.

B. EXPERMENTAL RESULTS

To confirm the workability of the proposed circuit, simulation and experiment tests have been performed simultaneously. The circuit was evaluated by PSPICE simulation and experiment test using commercial OTA LM13700. The DDTA is implemented using OTA LM13700 as shown in Fig. 18. The supply voltages were selected as $V_{DD} = -V_{DD} = 5$ V, the resistors $R_{ABC1} = R_{ABC2}$ were fixed as 47 kΩ and resistor R_{ABC3} was used to adjust the transconductance g_m of DDTA. The capacitances C_1 and C_2 were 22 nF for both filter and oscillator.

The sinusoidal input signal and the measured output waveforms were taken using Agilent Technologies DSO-X 2002A oscilloscope. The proposed universal filter was tested by setting the transconductances $g_{m1} = g_{m2} = g_{m3} =$ 1.5 mS ($g_m = I_{ABC}/2V_T$, I_{ABC} = 78.02 μA, $V_T \approx$ 26 mV) and the resistor R_1 = 660 Ω. This setting has been designed the. universal filter to obtain the natural frequency of

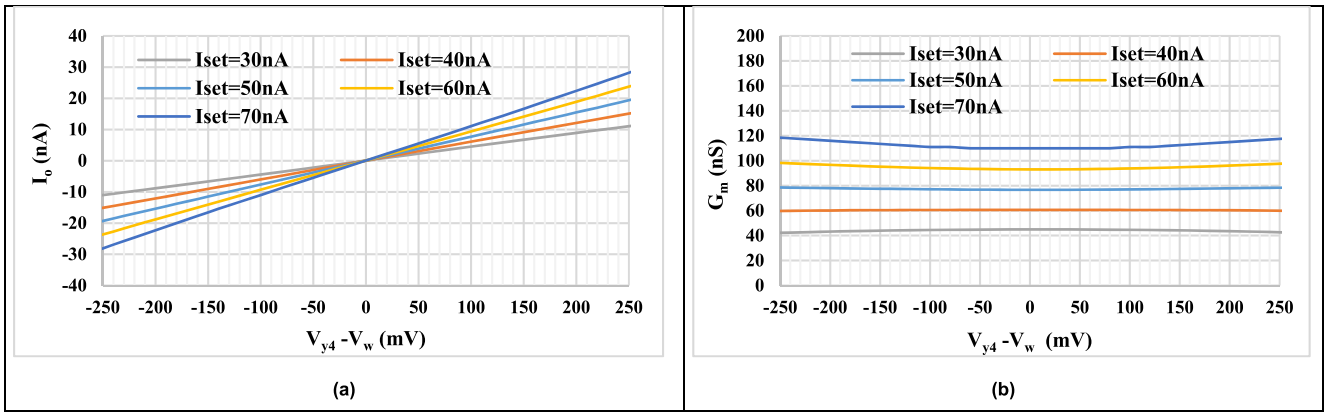

FIGURE 8. The relation of: a) I_o and b) G_m versus input voltage ($V_{y4} - V_w$) with different value of I_{set}.

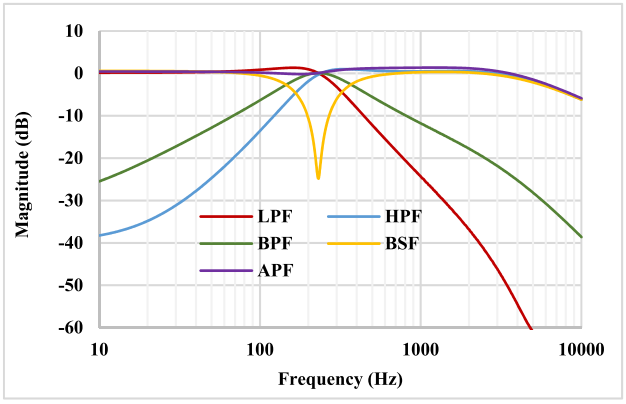

FIGURE 9. The frequency magnitude responses of LPF, HPF, BPF, BSF and APF.

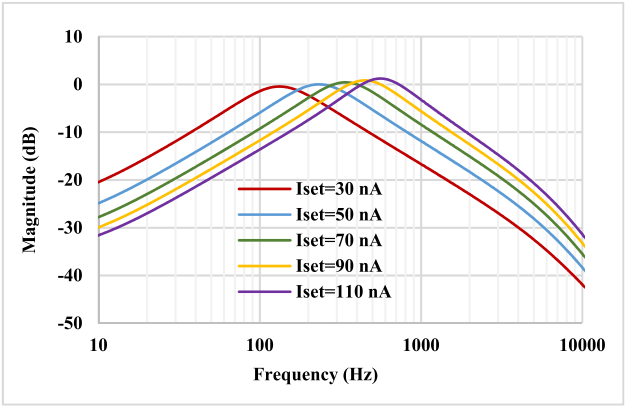

FIGURE 10. The frequency magnitude responses of BPF filter with different I_{set}.

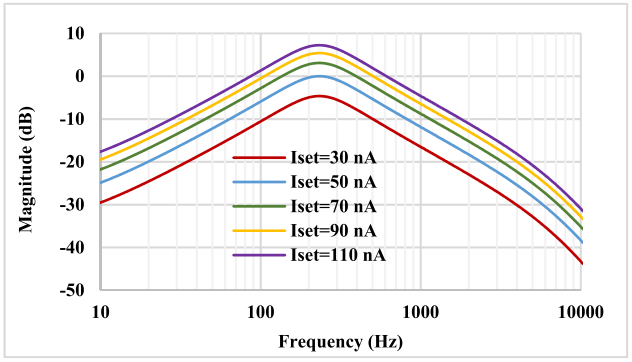

FIGURE 11. The frequency magnitude responses of BPF with different I_{set}.

$f_o = 10.85$ kHz, the quality factor of $Q \approx 1$, and the voltage gain of $H_o = 1$. The bias current I_{ABC} of 78.02 μA can be obtained by using the resistance of 47 kΩ (R_{ABC} =47 kΩ).

Fig. 19 shows magnitude responses of LPF, HPF, BPF, and BSF responses with natural frequency of $f_o = 10.85$ kHz. Fig. 20 shows magnitude and phase responses of AP filter. Figs. 19 and 20 confirm that the proposed filter provides five standard filtering responses.

Fig. 21 shows the magnitude responses of BP filters when the values of g_m ($g_m = g_{m1} = g_{m3}$) were 0.481 mS (I_{ABC} = 24.84 μA, R_{ABC} =150 kΩ), 0.873 mS (I_{ABC} = 45.06 μA, R_{ABC} = 82 kΩ), 1.512 mS (I_{ABC} = 78.02 μA, R_{ABC} = 47 kΩ), 2.934 mS (I_{ABC} = 151.4 μA, R_{ABC} = 24 kΩ) and 5.81 mS (I_{ABC} = 299.8 μA, R_{ABC} = 12 kΩ). The natural frequency f_o was 3.48 kHz, 6.31 kHz, 10.93 kHz, 21.22 kHz, and 42.03 kHz when g_m was changed respectively from 0.481 mS, 0.873 mS, 1.512 mS, 2.934 mS, and 5.81 mS, respectively. This result confirms eqn. (24), showing that the proposed filter enjoys electronic tuning ability.

Fig. 22 shows magnitude responses of LPF, HPF, BPF, BSF and APF at the natural frequency of $f_o = 10.85$ kHz with the voltage gain H_o =3 (≈9.5 dB). This result confirm that the voltage gain of the proposed filter can be adjusted (R_{ABC} = 15 kΩg_{m1} =4.627 mS)

The proposed quadrature oscillator was evaluated by PSPICE simulation and experiment test using commercial OTA LM13600. The supply voltages were $V_{DD} = -V_{DD}$ = 5 V and the capacitances C_1 and C_2 were 22 nF. The output waveforms were measured using Tektronix MSO 4034 mixed signal oscilloscope (4-channel oscilloscope).

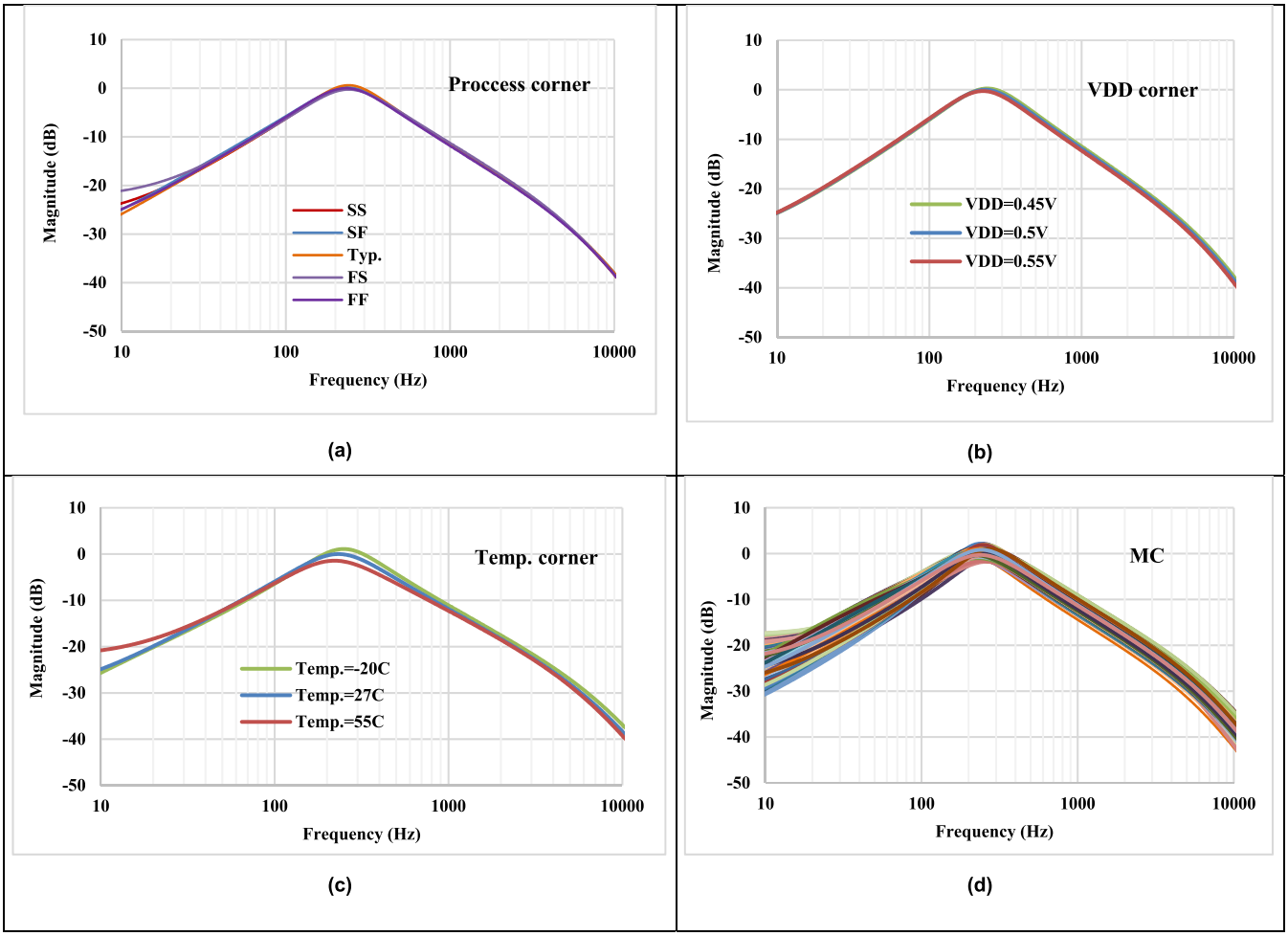

FIGURE 12. The frequency magnitude responses of BP filter with: a) proccess, b) VDD, c) temp. corners and d) MC analyses.

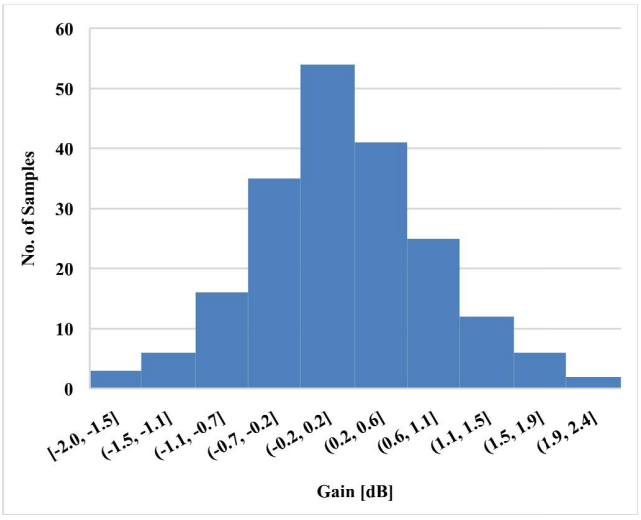

FIGURE 13. The histogram of the gain of the BP filter with 200 runs MC analysis.

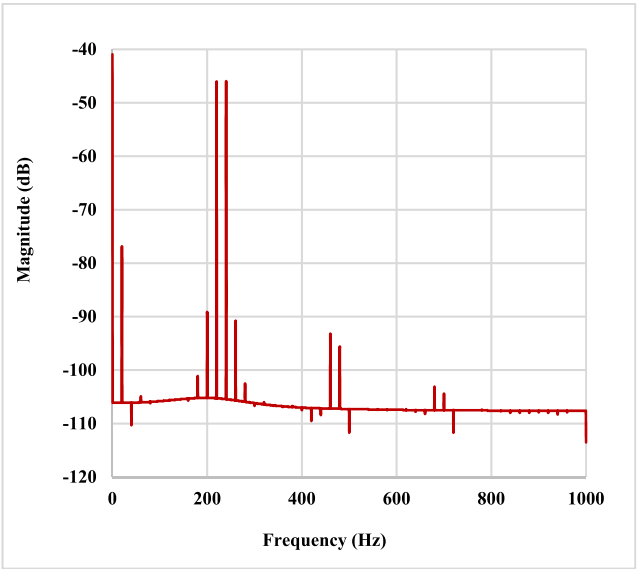

FIGURE 14. The spectrum of the output signal of the BP filter with two-tone test.

Fig. 23 shows the measured output wave forms of V_{o4} and V_{o5} for $g_{m1} = g_{m2} = 1.5$ mS and $R_1 = 660\ \Omega$ while g_{m3} was used to control the CO ($g_{m3} \cong 1.48$ mS). The circuit generates the signal of frequency of 9.67 kHz while theoretical value was 10.93 kHz.

TABLE 3. Performance comparison of this work with those of recently published.

Factor	[20]	[23]	[24]	[42]	[44]	[45]	[46]	Proposed
Number of active devices	4-OTA	3-CFOA	4-OTA	3-DDTA	2-DDTA	5-DDTA	8 OTA	3 DDTA
Realization	Com. IC	180 nm	180 nm	180 nm	130 nm	180 nm	180 nm	130 nm
Number of passive devices	2-C	2-C, 4-R	2-C	2-C	2-C	2-C	2-C, 1-R	2-C, 1-R
Type of filter	MIMO	MIMO	MISO	MIMO	MIMO	MIMO	MISO	MIMO
Operation mode	VM	VM	VM	VM	VM	MM	VM	VM
Number of offered responses	6	5	20	23	22	36	5	36
Orthogonal control of ω_o and Q	Yes	Yes	Yes	Yes	Yes	Yes	Yes	Yes
Offer voltage gain (H_o)	No	No	No	No	No	No	No	Yes
Electronic control of ω_o	Yes	No	Yes	Yes	Yes	Yes	Yes	Yes
Electronic control of H_o	No	No	No	No	No	No	No	Yes
Offer modified into oscillator	Yes	Yes	Yes	No	Yes	No	No	Yes
Orthogonal control of CO and FO	Yes	Yes	Yes	-	Yes	-	-	Yes
Electronic control of CO and FO	Yes	No	Yes	-	No	-	-	Yes
Natural frequency (Hz)	144.7×10^3	757.8×10^3	1000	254	81.47	1.04	10	231.7
Simulated power supply (V)	±15	±0.9	1.2	0.5	0.3	1.2	0.5	0.5
Power dissipation (μW)	0.92×10^6	4.8×10^3	96	0.616	0.715	0.33×10^3	0.0533	0.831
THD (%)	<1@55mV_{pp}	3.18@1.2 V_{pp}	1.67@600m V_{pp}	1.2@120m V_{pp}	0.5@100m V_{pp}	1.09@650m V_{pp}	1.0@200m V_{pp}	1.0@80mV_{pp}*
IRN ($\mu V/\sqrt{Hz}$)	-	-	-	116	-	150	-	61.37
Dynamic range (dB)	-	-	78.6	49.7	-	63.69	63	53.27
FOM (PD/(N×BW×DR) (pJ)**	-	-	610	24.39	-	2491	42.3	33.66
Verification of result	Sim/Exp	Sim/Exp	Sim/Exp	Sim	Sim	Sim/Exp	Sim	Sim

Note: * IMD_3- two tones test, ** PD=power dissipation, N=order of filter.

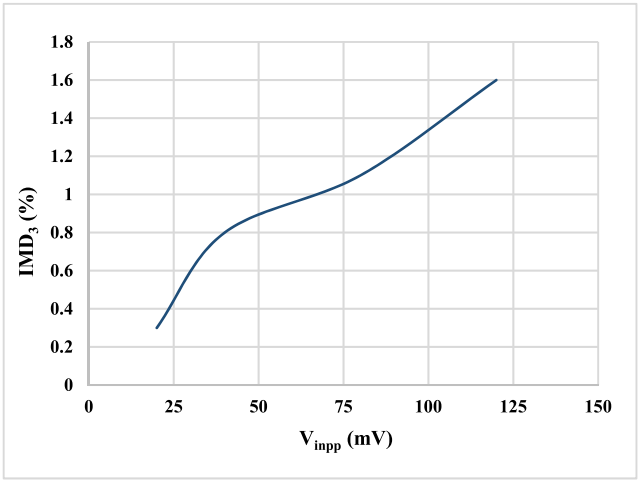

FIGURE 15. The IMD_3 of the BPF versus V_{inpp}.

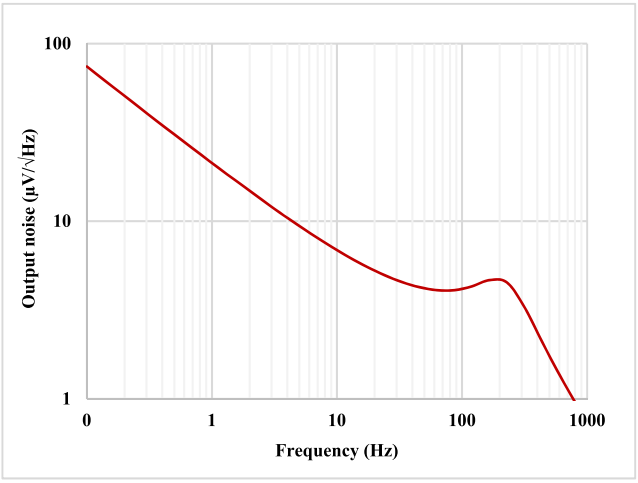

FIGURE 16. The output noise of the BPF.

Fig. 24 shows the quadrature output verifying through the X-Y mode. The measured result compared with the theoretical value of the FO by varying the value of transconductances g_{m2} was shown in Fig. 25. In this figure, when the transconductance g_{m2} was changed from 0.481 mS to 8.45 mS, the measured value of FO was changed respectively from 6.24 kHz to 25.21 kHz. Fig. 26 shows the plot for amplitude versus FO. It should be noted that the amplitude is not constant when g_{m2} was varied. The amplitude-automatic gain control (AGC) circuit [58] must be used if the constant

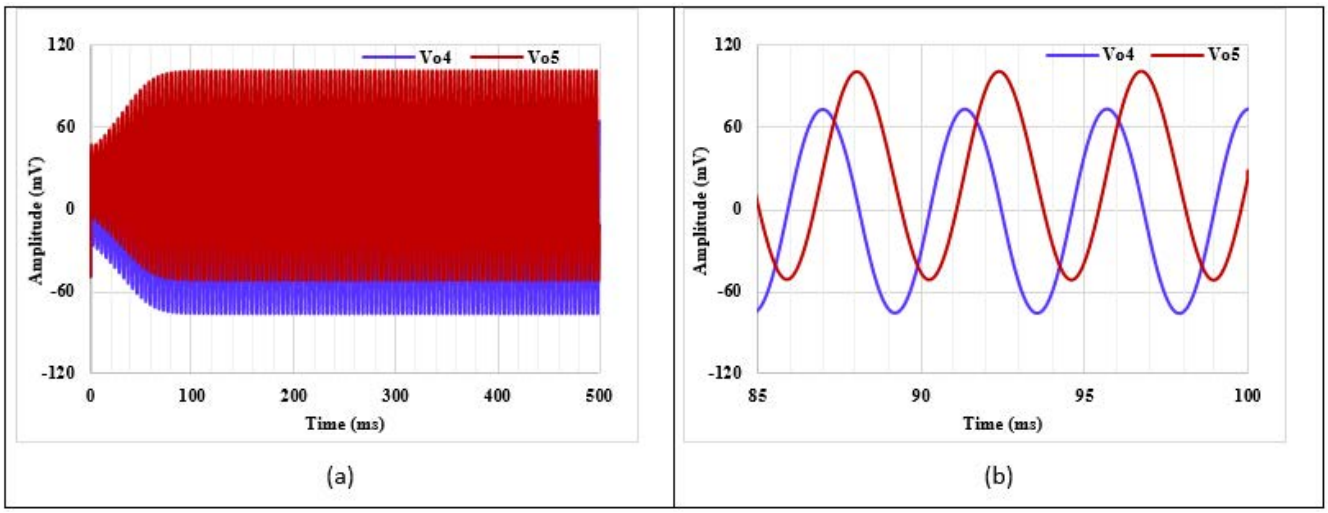

FIGURE 17. The starting the oscillation (a) and the steady state (b).

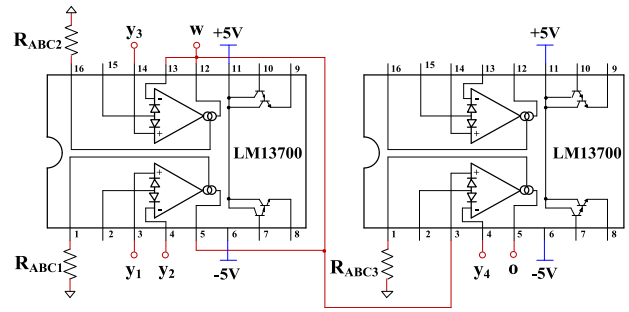

FIGURE 18. OTA LM3700-based DDTA for experiment test.

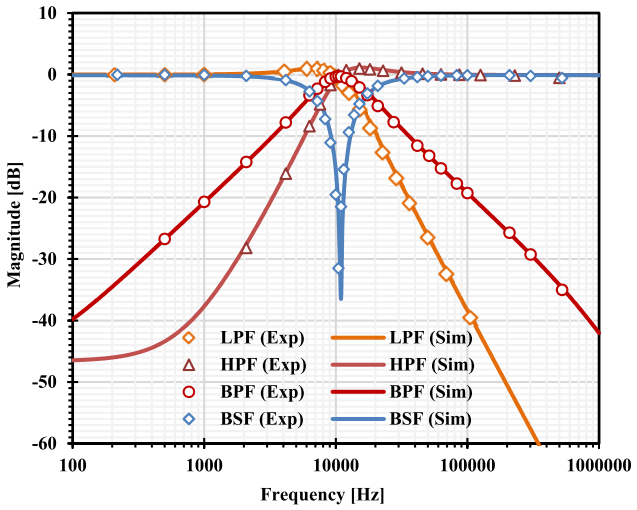

FIGURE 19. Measured magnitude response of LPF, HPF, BPF and BSF.

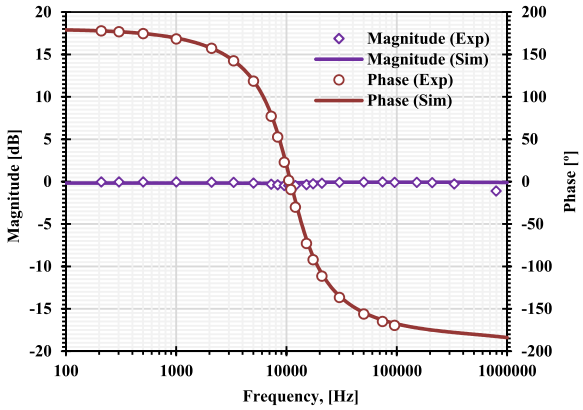

FIGURE 20. Measured magnitude and phase responses of APF.

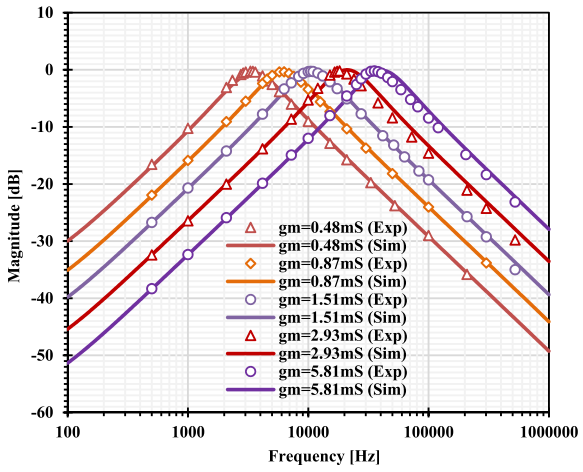

FIGURE 21. Measured magnitude response of BPF with different g_m.

amplitude of output signals is needed. Fig. 27 shows the phase error of outputs between V_{out1} and V_{out2} that is deviated from 90°. Finally, Fig. 28 shows the measured results of the frequency responses, Fig. 29 shows the breadboard implemented for the universal filter and Fig. 30 shows

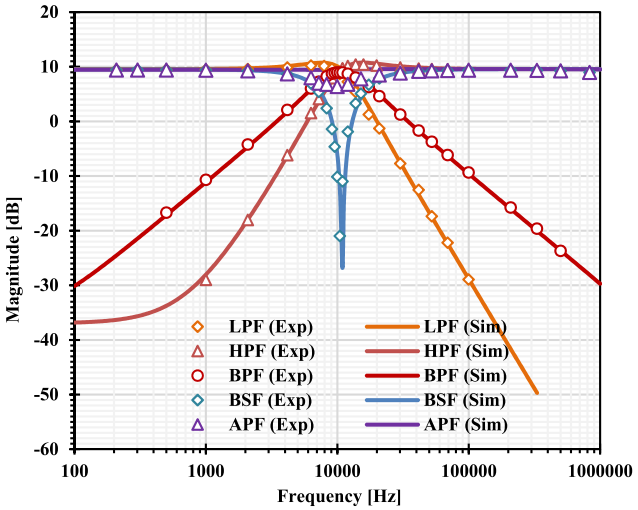

FIGURE 22. Measured magnitude response of LPF, HPF, BPF, BSF and APF with voltage gain 9.5 dB.

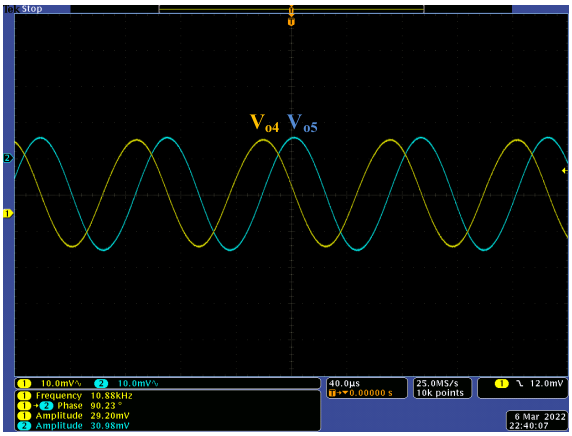

FIGURE 23. Measured output waveforms of V_{o4} and V_{o5}.

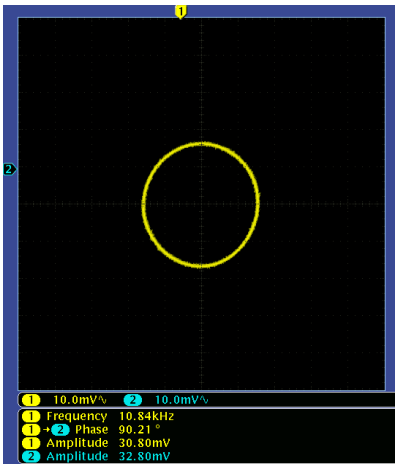

FIGURE 24. Measured results for X-Y plot of V_{o4} and V_{o5}.

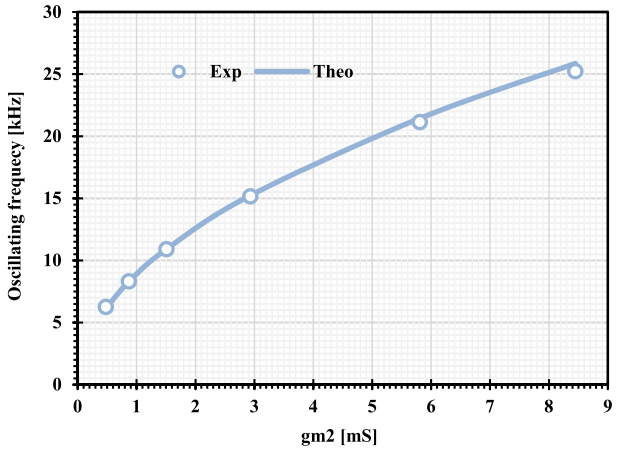

FIGURE 25. Measured oscillating frequency by varying g_{m2}.

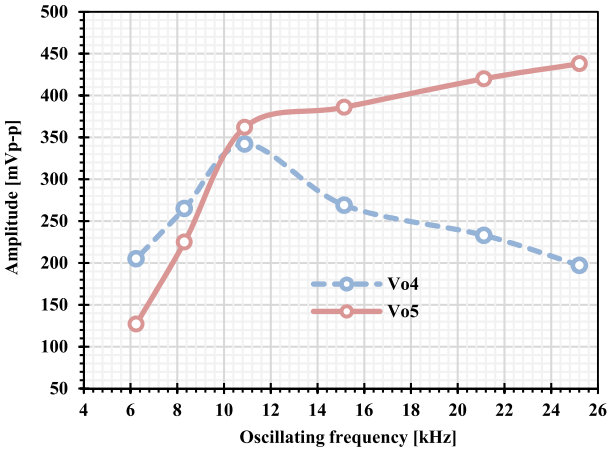

FIGURE 26. Measured amplitude of V_{o4} and V_{o5} when varying the oscillating frequency.

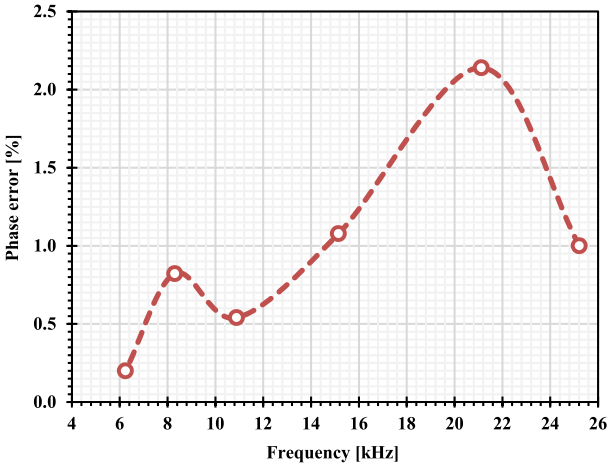

FIGURE 27. Measured results of phase error between V_{o4} and V_{o5}.

the experiment setup for the quadrature oscillator. It is worth noting that, the measured results are included in this work to confirm the functionality of the universal filter and oscillator in general also to show the advantages of the CMOS DDTA in form of reducing the count of active

FIGURE 28. **Measured frequency responses, a) LPF, b) HPF, c) BPF, d) BSF, e) APF and f) LPF with voltage gain greater than unity.**

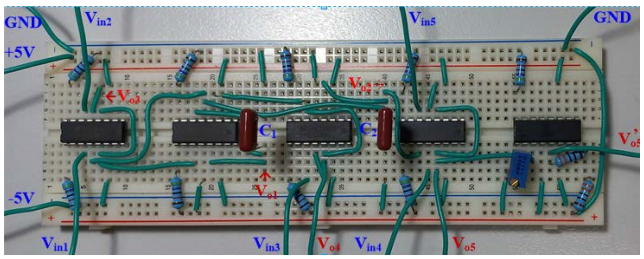

FIGURE 29. **The breadboard implemented the universal filter.**

blocks needed for the application realization, i.e. 3DDTAs versus 6 LM13700.

The performance of the proposed circuit and compared with some previous works has been summarized in Table 3. The circuits in [20], [23], [24], [42], [44], [45], [46] have been used for comparison. Compared with [20], [23], [24], the proposed circuit enjoys low-power consumption. Compared with [42], [45], [46], the proposed structure can realize both universal filter and quadrature oscillator. Compared with [24], [45], [46], the proposed circuit offers better figure of merit (FOM). Finally, compared with all circuits [20],[23], [24], [42], [44], [45], [46], the proposed filter offers the controlled voltage gain for both of the non-inverting and inverting of transfer function

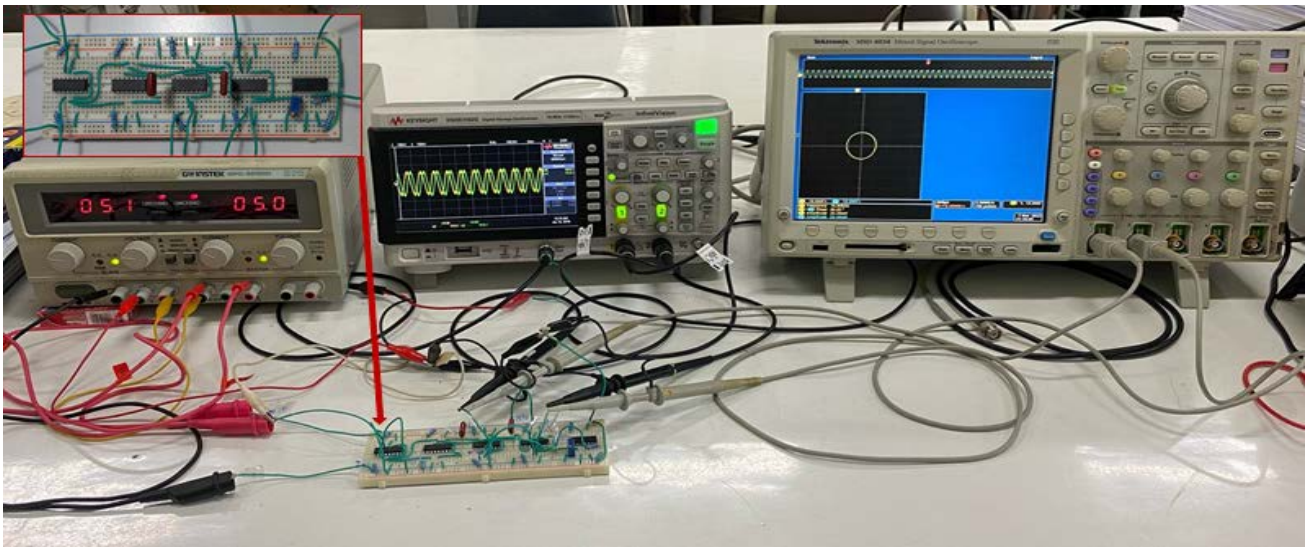

FIGURE 30. Experiment setup in case quadrature oscillator.

IV. CONCLUSION

The universal filter and quadrature oscillator using differential difference transconductance amplifier as active element for low frequency biomedical and biosensor applications has been presented in this paper. The proposed filter uses 0.5 V supply voltage and consumes 831 nW of power. The proposed universal filter provides thirty-six filtering functions of LPF, HPF, BPF, BSF and APF with

both inverting and non-inverting version, as well as both unity voltage gain and non-unity voltage gain. The natural frequency and quality factor can be orthogonally controlled. The natural frequency also enjoys electronic tuning ability. The quadrature oscillator can be realized from the proposed filter by slightly adding a connection. The condition and frequency of oscillations can be controlled electronically and orthogonally. The output impedance of the oscillator is low thus they can be connected to a load without buffer circuits.

REFERENCES

[1] L. W. Couch, *Digital and Analog Communication Systems*, 8th ed. London, U.K.: Pearson, 2013.

[2] M. A. Ibrahim, S. Minaei, and H. Kuntman, "A 22.5 MHz current-mode KHN-biquad using differential voltage current conveyor and grounded passive elements," *AEU-Int. J. Electron. Commun.*, vol. 59, no. 5, pp. 311–318, Jul. 2005, doi: 10.1016/j.aeue.2004.11.027.

[3] *MAX263*. Accessed: May 13, 2008. [Online]. Available: https://www.maximintegrated.com/en/products/analog/analog-filters/MAX263.html

[4] Y. Li, "Current-mode sixth-order elliptic band-pass filter using MCDTAs," *Radioengineering*, vol. 20, pp. 645–649, Sep. 2011.

[5] Y. Li, "A modified CDTA (MCDTA) and its applications: Designing current-mode sixth-order elliptic band-pass filter," *Circuits, Syst., Signal Process.*, vol. 30, no. 6, pp. 1383–1390, Dec. 2011.

[6] P. Prommee and E. Saising, "CMOS-based high-order LP and BP filters using biquad functions," *IET Circuits, Devices Syst.*, vol. 12, no. 4, pp. 326–334, Jul. 2018.

[7] M. Kumngern, T. Kulej, F. Khateb, V. Stopjakova, and R. K. Ranjan, "Nanopower multiple-input DTMOS OTA and its applications to high-order filters for biomedical systems," *AEU-Int. J. Electron. Commun.*, vol. 130, Feb. 2021, Art. no. 153576.

[8] B. Razavi, *Design of CMOS Phase-Locked Loops*, 1st ed. Cambridge, U.K.: Cambridge Univ. Press, 2020.

[9] L. B. Oliveira, J. R. Fernandes, I. M. Filanovsky, C. J. M. Verhoeven, and M. M. Silva, *Analysis and Design of Quadrature Oscillators*. Dordrecht, The Netherlands: Springer, 2010.

[10] W. Jaikla, S. Adhan, P. Suwanjan, and M. Kumngern, "Current/voltage controlled quadrature sinusoidal oscillators for phase sensitive detection using commercially available IC," *Sensors*, vol. 20, no. 5, p. 1319, Feb. 2020.

[11] J.-W. Horng, "Quadrature oscillators using operational amplifiers," *Act. Passive Electron. Compon.*, vol. 2011, pp. 1–4, Jan. 2011, doi: 10.1155/2011/320367.

[12] W. Jaikla, M. Siripruchyanun, and A. Lahiri, "Resistorless dual-mode quadrature sinusoidal oscillator using a single active building block," *Microelectron. J.*, vol. 42, no. 1, pp. 135–140, 2011, doi: 10.1016/j.mejo.2010.08.017.

[13] M. Gupta and T. S. Arora, "Realization of current mode universal filter and a dual-mode single resistance controlled quadrature oscillator employing VDCC and only grounded passive elements," *Adv. Electr. Electron. Eng.*, vol. 15, no. 5, pp. 833–845, Jan. 2018, doi: 10.15598/aeee.v15i5.2397.

[14] M. Gupta and T. S. Arora, "Various applications of analog signal processing employing voltage differencing current conveyor and only grounded passive elements: A re-convertible approach," *Social Netw. Appl. Sci.*, vol. 2, no. 9, pp. 1–18, Sep. 2020, doi: 10.1007/s42452-020-03379-6.

[15] Y. A. Li, "Electronically tunable current-mode biquadratic filter and four-phase quadrature oscillator," *Microelectron. J.*, vol. 45, no. 3, pp. 330–335, Mar. 2014, doi: 10.1016/j.mejo.2013.12.005.

[16] W. Tangsrirat, T. Pukkalanun, and O. Channumsin, "Single VDGA-based dual-mode multifunction biquadratic filter and quadrature sinusoidal oscillator," *J. Microelectron., Electron. Compon. Mater.*, vol. 50, no. 2, pp. 125–136, 2020, doi: 10.33180/InfMIDEM2020.205.

[17] S.-F. Wang, H.-P. Chen, Y. Ku, and C.-M. Yang, "A voltage-mode universal filter using five single-ended OTAs with two grounded capacitors and a quadrature oscillator using the voltage-mode universal filter," *Optik*, vol. 192, Sep. 2019, Art. no. 162950.

[18] S.-F. Wang, H.-P. Chen, Y. Ku, and C.-M. Yang, "Independently tunable voltage-mode OTA-C biquadratic filter with five inputs and three outputs and its fully-uncoupled quadrature sinusoidal oscillator application," *AEU-Int. J. Electron. Commun.*, vol. 110, Oct. 2019, Art. no. 152822.

[19] S.-F. Wang, H.-P. Chen, Y. Ku, and Y.-C. Lin, "Versatile tunable voltage-mode biquadratic filter and its application in quadrature oscillator," *Sensors*, vol. 19, no. 10, p. 2349, May 2019.

[20] S.-F. Wang, H.-P. Chen, Y. Ku, and C.-L. Lee, "Versatile voltage-mode biquadratic filter and quadrature oscillator using four OTAs and two grounded capacitors," *Electronics*, vol. 9, no. 9, p. 1493, Sep. 2020.

[21] S.-F. Wang, H.-P. Chen, Y. Ku, and M.-X. Zhong, "Voltage-mode multifunction biquad filter and its application as fully-uncoupled quadrature oscillator based on current-feedback operational amplifiers," *Sensors*, vol. 20, no. 22, p. 6681, Nov. 2020, doi: 10.3390/s20226681.

[22] S.-F. Wang, H.-P. Chen, Y. Ku, and P.-Y. Chen, "A CFOA-based voltage-mode multifunction biquadratic filter and a quadrature oscillator using the CFOA-based biquadratic filter," *Appl. Sci.*, vol. 9, no. 11, p. 2304, Jun. 2019, doi: 10.3390/app9112304.

[23] S.-F. Wang, H.-P. Chen, Y. Ku, and M.-X. Zhong, "Analytical synthesis of high-pass, band-pass and low-pass biquadratic filters and its quadrature oscillator application using current-feedback operational amplifiers," *IEEE Access*, vol. 9, pp. 13330–13343, 2021.

[24] S.-F. Wang, H.-P. Chen, Y. Ku, and F.-Y. Liu, "Design and experiment of electronically tunable voltage-mode biquad and output current amplitude oscillator," *Appl. Sci.*, vol. 11, no. 16, p. 7357, Aug. 2021, doi: 10.3390/app11167357.

[25] S.-F. Wang, H.-P. Chen, Y. Ku, and W.-Y. Chen, "Isomorphic circuits of independent amplitude tunable voltage-mode bandpass filters and quadrature sinusoidal oscillators," *Appl. Sci.*, vol. 11, no. 16, p. 7431, Aug. 2021, doi: 10.3390/app11167431.

[26] S.-F. Wang, H.-P. Chen, Y. Ku, and C.-L. Lee, "Voltage-mode biquad filter using four OTAs and its application in quadrature oscillator with noninteractive control of the oscillation condition and frequency," *J. Circuits, Syst. Comput.*, vol. 31, no. 4, 2022, Art. no. 2250078, doi: 10.1142/S0218126622500773.

[27] M. Siripruchyanun and W. Jaikla, "Cascadable current-mode biquad filter and quadrature oscillator using DO-CCCIIs and OTA," *Circuits, Syst. Signal Process.*, vol. 28, no. 1, pp. 99–110, Feb. 2009, doi: 10.1007/s00034-008-9072-5.

[28] H.-P. Chen, Y.-S. Hwang, Y.-T. Ku, S.-F. Wang, and C.-H. Wu, "Voltage-mode universal biquadratic filter and quadrature oscillator using CFAs," *IEICE Electron. Exp.*, vol. 13, no. 15, pp. 1–11, 2016, doi: 10.1587/elex.13.20160510.

[29] M. Kumngern, E. Wareechol, and P. Phasukkit, "Quadrature oscillator and universal filter based on translinear current conveyors," *AEU-Int. J. Electron. Commun.*, vol. 94, pp. 69–78, Sep. 2018, doi: 10.1016/j.aeue.2018.06.044.

[30] M. Kumngern and F. Khateb, "Current-mode universal filter and quadrature oscillator using current controlled current follower transconductance amplifiers," *Anal. Integr. Circuits Signal Process.*, vol. 100, no. 2, pp. 235–248, Aug. 2019, doi: 10.1007/s10470-018-1345-8.

[31] B. Knobnob, U. Torteanchai, and M. Kumngern, "Programmable universal filter and quadrature oscillator using single output operational transconductance amplifiers," *J. Microelectron., Electron. Compon. Mater.*, vol. 51, pp. 225–241, Dec. 2021.

[32] T. T. Zhang, P.-I. Mak, M.-I. Vai, P.-U. Mak, M.-K. Law, S.-H. Pun, F. Wan, and R. P. Martins, "15-nW biopotential LPFs in 0.35-μm CMOS using subthreshold-source-follower biquads with and without gain compensation," *IEEE Trans. Biomed. Circuits Syst.*, vol. 7, no. 5, pp. 690–702, Oct. 2013.

[33] S. Thanapitak and C. Sawigun, "A subthreshold buffer-based biquadratic cell and its application to biopotential filter design," *IEEE Trans. Circuits Syst. I, Reg. Papers*, vol. 65, no. 9, pp. 2774–2783, Sep. 2018.

[34] C. Sawigun and S. Thanapitak, "A 0.9-nW, 101-Hz, and 46.3-μV_{rms} IRN low-pass filter for ECG acquisition using FVF biquads," *IEEE Trans. Very Large Scale Integr. (VLSI) Syst.*, vol. 26, no. 11, pp. 2290–2298, Nov. 2018.

[35] V. S. Rajan, K. H. Kishore, R. Sanjay, S. Kumaravel, and B. Venkataramani, "A novel programmable attenuator based low G_m-OTA for biomedical applications," *Microelectron. J.*, vol. 97, Mar. 2020, Art. no. 104721.

[36] M. Yang, J. Liu, Y. Xiao, and H. Liao, "14.4 nW fourth order bandpass filter for biomedical applications," *Electron. Lett.*, vol. 16, no. 14, pp. 973–974, 2010.

[37] C. Sawigun, W. Ngamkham, and W. A. Serdijn, "A 0.5-V, 2-nW, 55-dB DR, fourth-order bandpass filter using single branch biquads: An efficient design for FoM enhancement," *Microelectron. J.*, vol. 45, no. 4, pp. 367–374, Apr. 2014.

[38] Y. Sundarasaradula and A. Thanachayanont, "A 1-V, 6-nW programmable 4th-order bandpass filter for biomedical applications," *Anal. Integr. Circuits Signal Process.*, vol. 89, no. 1, pp. 89–98, Oct. 2016.

[39] C. Hwang, S. Bibyk, M. Ismail, and B. Lohiser, "A very low frequency, micropower, low voltage CMOS oscillator for noncardiac pacemakers," *IEEE Trans. Circuits Syst. I, Fundam. Theory Appl.*, vol. 42, no. 11, pp. 962–966, Nov. 1995, doi: 10.1109/81.477208.

[40] I. A. A. Al-Darkazly and S. M. R. Hasan, "Dual-band waveform generator with ultra-wide low-frequency tuning-range," *IEEE Access*, vol. 4, pp. 3169–3181, 2016, doi: 10.1109/ACCESS.2016.2557843.

[41] M. Mohsen, L. A. Said, A. S. Elwakil, A. H. Madian, and A. G. Radwan, "Extracting optimized bio-impedance model parameters using different topologies of oscillators," *IEEE Sensors J.*, vol. 20, no. 17, pp. 9947–9954, Sep. 2020.

[42] F. Khateb, M. Kumngern, T. Kulej, and D. Biolek, "0.5 V differential difference transconductance amplifier and its application in voltage-mode universal filter," *IEEE Access*, vol. 10, pp. 43209–43220, 2022, doi: 10.1109/ACCESS.2022.3167700.

[43] M. Kumngern, F. Khateb, T. Kulej, and C. Psychalinos, "Multiple-input universal filter and quadrature oscillator using multiple-input operational transconductance amplifiers," *IEEE Access*, vol. 9, pp. 56253–56263, 2021.

[44] F. Khateb, M. Kumngern, T. Kulej, and D. Biolek, "0.3-volt rail-to-rail DDTA and its application in a universal filter and quadrature oscillator," *Sensors*, vol. 22, no. 7, p. 2655, Mar. 2022, doi: 10.3390/s22072655.

[45] M. Kumngern, P. Suksaibul, F. Khateb, and T. Kulej, "1.2 V differential difference transconductance amplifier and its application in mixed-mode universal filter," *Sensors*, vol. 22, no. 9, p. 3535, May 2022, doi: 10.3390/s22093535.

[46] W. Jaikla, F. Khateb, M. Kumngern, T. Kulej, R. K. Ranjan, and P. Suwanjan, "0.5 V fully differential universal filter based on multiple input OTAs," *IEEE Access*, vol. 8, pp. 187832–187839, 2020, doi: 10.1109/ACCESS.2020.3030239.

[47] J. Yan and R. L. Geiger, "A negative conductance voltage gain enhancement technique for low voltage high speed CMOS op amp design," in *Proc. 43rd IEEE Midwest Symp. Circuits Syst.*, Aug. 2000, pp. 502–505, doi: 10.1109/MWSCAS.2000.951693.

[48] T. Kulej, "0.5-V bulk-driven CMOS operational amplifier," *IET Circuits, Devices Syst.*, vol. 7, no. 6, pp. 352–360, Nov. 2013, doi: 10.1049/iet-cds.2012.0372.

[49] T. Kulej, "0.4-V bulk-driven operational amplifier with improved input stage," *Circuits, Syst., Signal Process.*, vol. 34, no. 4, pp. 1167–1185, Apr. 2015, doi: 10.1007/s00034-014-9906-2.

[50] T. Kulej and F. Khateb, "Design and implementation of sub 0.5-V OTAs in 0.18-μm CMOS," *Int. J. Circuit Theory Appl.*, vol. 46, no. 6, pp. 1129–1143, Jun. 2018, doi: 10.1002/cta.2465.

[51] F. Khateb, T. Kulej, M. Kumngern, and C. Psychalinos, "Multiple-input bulk-driven MOS transistor for low-voltage low-frequency applications," *Circuits, Syst., Signal Process.*, vol. 38, no. 6, pp. 2829–2845, Jun. 2019.

[52] F. Khateb, T. Kulej, M. Kumngern, D. Arbet, and W. Jaikla, "A 0.5-V 95-dB rail-to-rail DDA for biosignal processing," *AEU-Int. J. Electron. Commun.*, vol. 145, pp. 1–9, Feb. 2022, doi: 10.1016/j.aeue.2021.154098.

[53] T. Kulej, F. Khateb, D. Arbet, and V. Stopjakova, "A 0.3-V high linear rail-to-rail bulk-driven OTA in 0.13 μm CMOS," *IEEE Trans. Circuits Syst. II, Exp. Briefs*, vol. 69, no. 4, pp. 2046–2050, Apr. 2022, doi: 10.1109/TCSII.2022.3144095.

[54] A. J. Lopez-Martin, S. Baswa, J. Ramirez-Angulo, and R. G. Carvajal, "Low-voltage super class AB CMOS OTA cells with very high slew rate and power efficiency," *IEEE J. Solid-State Circuits*, vol. 40, no. 5, pp. 1068–1077, May 2005, doi: 10.1109/JSSC.2005.845977.

[55] C. Galup-Montoro, M. C. Schneider, and I. J. B. Loss, "Series-parallel association of FET's for high gain and high frequency applications," *IEEE J. Solid-State Circuits*, vol. 29, no. 9, pp. 1094–1101, Sep. 1994.

[56] T. Tsukutani, M. Higashimura, N. Takahashi, Y. Sumi, and Y. Fukui, "Versatile voltage-mode active-only biquad with lossless and lossy integrator loop," *Int. J. Electron.*, vol. 88, pp. 1093–1102, Oct. 2001, doi: 10.1080/00207210110071279.

[57] G. Daryanani, *Principle of Active Network Synthesis and Analysis*. New York, NY, USA: Willy, 1976.

[58] R. Sotner, J. Jerabek, L. Langhammer, J. Polak, N. Herencsar, R. Prokop, J. Petrzela, and W. Jaikla, "Comparison of two solutions of quadrature oscillators with linear control of frequency of oscillation employing modern commercially available devices," *Circuit, Syst. Signal Process.*, vol. 34, no. 11, pp. 3449–3469, 2015, doi: 10.1007/s00034-015-0015-7.

[59] C. D. Salthouse and R. Sarpeshkar, "A practical micropower programmable bandpass filter for use in bionic ears," *IEEE J. Solid-State Circuits*, vol. 38, no. 1, pp. 63–70, Jan. 2003, doi: 10.1109/JSSC.2002.806286.

[60] S. A. Mahmoud, A. Bamakhramah, and S. A. Al-Tunaiji, "Six order cascaded power line notch filter for ECG detection systems with noise shaping," *Circuits, Syst., Signal Process.*, vol. 33, no. 8, pp. 2385–2400, Aug. 2014, doi: 10.1007/s00034-014-9761-1.

[61] L. P. L. van Dijk, A. C. van der Woerd, J. Mulder, and A. H. M. van Roermund, "An ultra-low-power, low-voltage electronic audio delay line for use in hearing aids," *IEEE J. Solid-State Circuits*, vol. 33, no. 2, pp. 291–294, Feb. 1998, doi: 10.1109/4.658633.
[62] W. Wu, Y. Gil, and J. Lee, "Combination of wearable multi-biosensor platform and resonance frequency training for stress management of the unemployed population," *Sensors*, vol. 12, no. 10, pp. 13225–13248, Oct. 2012, doi: 10.3390/s121013225.
[63] J. R. Aggas, E. Sánchez-Sinencio, and A. Guiseppi-Elie, "Wien oscillator using organic enzyme-chemiresistors for fused measurement of glucose and lactate," *Adv. Intell. Syst.*, vol. 2, no. 7, Jul. 2020, Art. no. 2000004, doi: 10.1002/aisy.202000004.
[64] J. H. Kim, S. J. Park, J.-W. Han, and J.-H. Ahn, "Surface potential-controlled oscillation in FET-based biosensors," *Sensors*, vol. 21, no. 6, p. 1939, Mar. 2021, doi: 10.3390/s21061939.

MONTREE KUMNGERN received the B.S.Ind.Ed. degree in electrical engineering from the King Mongkut's University of Technology Thonburi, Thailand, in 1998, and the M.Eng. and D.Eng. degrees in electrical engineering from the King Mongkut's Institute of Technology Ladkrabang, Thailand, in 2002 and 2006, respectively. In 2007, he worked as a Lecturer with the Department of Telecommunications Engineering, Faculty of Engineering, King Mongkut's Institute of Technology Ladkrabang. From 2010 to 2017, he worked as an Assistant Professor. He is currently an Associate Professor. He has authored or coauthored over 200 publications in journals and proceedings of international conferences. His research interests include analog and digital integrated circuits, discrete-time analog filters, non-linear circuits, data converters, and ultra-low voltage building blocks for biomedical applications.

PICHAI SUKSAIBUL received the B.Eng. and M.Eng. degrees from the Rajamangala University of Technology Thanyaburi, Thailand, in 2014 and 2016, respectively. He is currently pursuing the D.Eng. degree in electrical engineering with the School of Engineering, King Mongkut's Institute of Technology Ladkrabang, Thailand. His research interests include analog and integrated circuit design.

FABIAN KHATEB received the M.Sc. degree in electrical engineering and communication, the M.Sc. degree in business and management, the Ph.D. degree in electrical engineering and communication, and the Ph.D. degree in business and management from the Brno University of Technology, Czech Republic, in 2002, 2003, 2005, and 2007, respectively. He is currently a Professor with the Department of Electrical Engineering, University of Defence, Brno (UDB), the Department of Microelectronics, Faculty of Electrical Engineering and Communication, Brno University of Technology, and the Department of Information and Communication Technology in Medicine, Faculty of Biomedical Engineering, Czech Technical University in Prague. He holds five patents. He has authored or coauthored over 100 publications in journals and proceedings of international conferences. He has expertise in new principles of designing low-voltage low-power analog circuits, particularly biomedical applications. He is a member of the Editorial Board of *Microelectronics Journal*, *Sensors*, *Electronics*, and *Journal of Low Power Electronics and Applications*. He is an Associate Editor of IEEE Access, *Circuits, Systems and Signal Processing*, *IET Circuits, Devices & Systems*, and *International Journal of Electronics*. He was a Lead Guest Editor for the special issues on Low Voltage Integrated Circuits and Systems on Circuits, Systems and Signal Processing, in 2017, *IET Circuits Devices & Systems*, in 2018, and *Microelectronics Journal*, in 2019. He was also a Guest Editor for the special issue on Current-Mode Circuits and Systems; Recent Advances, Design and Applications on *International Journal of Electronics and Communications*, in 2017.

TOMASZ KULEJ received the M.Sc. and Ph.D. degrees from the Gdańsk University of Technology, Gdańsk, Poland, in 1990 and 1996, respectively. He was a Senior Design Analysis Engineer at Polish Branch of Chipworks Inc., Ottawa, Canada. He is currently an Associate Professor with the Department of Electrical Engineering, Częstochowa University of Technology, Poland, where he conducts lectures on electronics fundamentals, analog circuits, and computer aided design. He has authored or coauthored over 90 publications in peer-reviewed journals and conferences. He holds three patents. His recent research interests include analog integrated circuits in CMOS technology, with emphasis to low voltage and low power solutions. He serves as an Associate Editor of the *Circuits Systems and Signal Processing* and *IET Circuits Devices and Systems*. He was also a Guest Editor for the special issues on Low Voltage Integrated Circuits on Circuits Systems and Signal Processing, in 2017, *IET Circuits Devices and Systems*, in 2018, and *Microelectronics Journal*, in 2019.